Journal of Chromatography, 142 (1977) 155–166

CHROM. 10,428

AXIAL DISPERSION OF GASES FLOWING THROUGH COILED COLUMNS

J. A. MOULIJN, R. SPIJKER and J. F. M. KOLK
Institute for Chemical Technology, University of Amsterdam, Plantage Muidergracht 30, Amsterdam (The Netherlands)

SUMMARY

A study is reported on the axial dispersion of gases in coiled tubes under laminar flow conditions. At low velocities coiled tubes and straight tubes show identical dispersion behaviour. At high velocities dispersion in coiled tubes is much less than in straight tubes. The dispersion coefficients measured are correlated in terms of dimensionless groups. The reduction in dispersion coefficient and, therefore, in the height equivalent to a theoretical plate, amounts to a factor of 10.

INTRODUCTION

Coiled tubes are widely used both in industry and in the laboratory; examples are heat exchangers and columns for gas chromatography. In comparison with straight tubes they offer the advantages of compactness, increased rates of heat and mass transfer and reduced axial dispersion. Many studies have been reported, from which conclusions can be drawn about flow characteristics and dispersion behaviour[1–12]. The increases in the rates of heat and mass transfer and the reduction in axial dispersion are caused by radial convective transport due to the so-called secondary flow. This reasoning is analogous to the narrowing of the residence time distribution due to radial diffusion in the Taylor–Aris model[13,14]. Most of the experimental work published so far has been carried out with liquid systems, probably because in engineering practice the flow of liquids is generally more important than the flow of gases. Moreover, secondary flow phenomena are more easily measurable in liquid systems. Nevertheless, the flow of gases is very interesting from a practical and theoretical point of view. A field where secondary flow of gases is certainly important is capillary gas chromatography. Coiled tubes are often also used for the measurement of molecular diffusion coefficients, while in general the assumption is made that the relationships for straight tubes hold.

The purpose of this study was to investigate gaseous dispersion in coiled tubes in order to establish whether for gases secondary flow effects are also measurable under conditions of practical interest and, if so, which parameters are important in quantitative correlations.

THEORETICAL

For a complete treatment of the influence of secondary flow on the residence time distribution, the continuity equation has to be solved in relation to the equations of motion, which is a very complex problem. In the literature two approaches have been followed. One approach consists in obtaining analytical solutions that are valid with certain approximations[1,4], while other workers have reported numerical solutions[5]. From the theoretical and experimental studies it can be concluded that, in principle, the dispersion observed in a coiled tube results from three mechanisms:

(1) the differences of the mean velocities of the various streams;
(2) molecular diffusion;
(3) secondary flow.

In this study, it was assumed that laminar flow conditions prevail, so that turbulence is not taken into account. As the laminar flow regime in helical tubes is much larger than in straight tubes, this is not a serious limitation in many applications.

In straight tubes, only the first two mechanisms are relevant. The velocity distribution in straight tubes is parabolic. Taylor[13] showed that for straight circular tubes the process of mass transfer resulting from the parabolic velocity distribution accompanied by molecular diffusion can be described by a dispersion model with a constant velocity and an axial dispersion coefficient. The mass balance for this model is

$$\frac{\partial c}{\partial t} + v\frac{\partial c}{\partial z} = \mathscr{D}\frac{\partial^2 c}{\partial z^2} \tag{1}$$

According to Taylor's treatment, this velocity is equal to the actual mean velocity and the axial dispersion coefficient has the form

$$\mathscr{D} = \frac{v^2 d^2}{192\, D_{1,2}} \tag{2}$$

where

$\mathscr{D}$ = dispersion coefficient ($m^2\ sec^{-1}$);
v = mean linear velocity ($m\ sec^{-1}$);
d = diameter of tube (m);
$D_{1,2}$ = binary molecular diffusion coefficient ($m^2\ sec^{-1}$).

In his solution, Taylor neglected axial molecular diffusion. Aris[14] showed that axial molecular diffusion can be incorporated in the model of Taylor simply by adding the molecular diffusion coefficient to the dispersion coefficient calculated by Taylor:

$$\mathscr{D} = \frac{v^2 d^2}{192\, D_{1,2}} + D_{1,2} \tag{3}$$

In any curved tube, secondary flow will develop owing to centrifugal forces. As the axial velocity depends on the radial position, the centrifugal force will also depend on the radial position. The fluid in the centre of the tube has the highest velocity and therefore will be thrown outwards. Of course, no accumulation of mass can take place and therefore the outward flow will be balanced by a flow inwards. In consequence, a

secondary flow develops in which the fluid in the centre moves outwards and the fluid near the bottom and the top moves inwards. The resulting flow is a double helix, as is shown in Fig. 1. The existence of this type of flow has been well documented[15]. Also in this Institute we have visualized this type of secondary flow in a liquid system as well as in a gas system. In curved tubes the velocity distribution cannot be described by a simple parabolic function and the flow profile will be asymmetric, especially at higher velocities[5].

The dispersion coefficients observed in coiled tubes will be interpreted by comparison with theoretical dispersion coefficients predicted by the Taylor–Aris model. It is convenient to use dimensionless quantities. For the definition of a dimensionless dispersion coefficient we follow the choice of Trivedi and Vasudeva[6]:

$$K = \frac{\mathscr{D}\, D_{1,2}}{v^2\, d^2} \tag{4}$$

The Taylor–Aris equation then reads

$$K_s = \frac{1}{192} + \frac{D_{1,2}^2}{v^2\, d^2} = \frac{1}{192} + \frac{1}{Pe_{1,2}^2} \tag{5}$$

where K_s is the dimensionless dispersion coefficient for straight tubes and $Pe_{1,2}$ is the Peclet group.

The experimental results with the coiled tubes will be interpreted in terms of deviations from the Taylor–Aris model:

$$K_c = K_s + \text{correction term} \tag{6}$$

where K_c is the dimensionless dispersion coefficient for coiled tubes and K_s is the dimensionless dispersion coefficient for straight tubes. From the literature, it can be concluded that this correction term is a function of the Reynolds group (Re), the Schmidt group (Sc) and the curvature ratio (λ). These three dimensionless groups are defined as

$$Re = \frac{vd}{\nu} \tag{7}$$

$$Sc = \frac{\nu}{D_{1,2}} \tag{8}$$

$$\lambda = \frac{d_c}{d} \tag{9}$$

where

ν = kinematic viscosity ($m^2\ sec^{-1}$);

d_c = coil diameter (m).

It has been shown that under certain conditions Re and λ are not independent variables, but the combination $Re/\sqrt{\lambda}$ determines the dispersion behaviour. This combination is called the Dean group (De). Moreover, with certain assumptions it

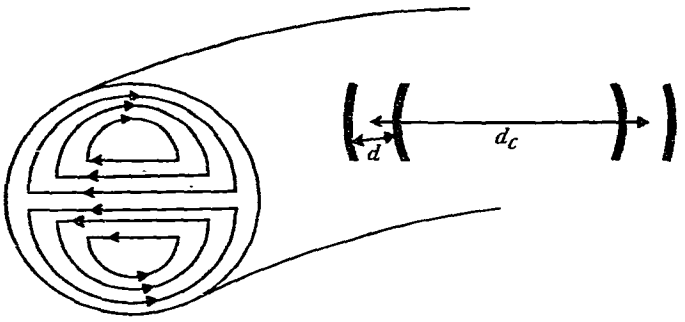

Fig. 1. Schematic secondary flow pattern in helical tubes and definition of coil diameter and tube diameter.

has been shown that secondary flow is completely characterized by the combination De^2Sc (ref. 10). This result is conceivable because the centrifugal force is characterized by De^2Sc.

In this treatment, it has been assumed that the axial dispersion model defined by eqn. 1 is also valid for coiled tubes, the only difference being a different dispersion coefficient. By Laplace transformation it can be simply proved that the parameters in eqn. 1, v and $\mathscr{D}$, are related to the first moment on the origin and second moment on the mean:

$$\mu_1 = \frac{L}{v} \tag{10}$$

$$\mu_2' = \frac{2\mathscr{D}L}{v^3} \tag{11}$$

where

$$\mu_1 = \int_0^\infty c\,t\,\mathrm{d}t = \text{first moment on the origin;}$$

$$\mu_2' = \int_0^\infty c\,(t-\mu_1)^2\,\mathrm{d}t = \text{second moment on the mean,}$$

while the concentration c has been normalized according to

$$\int_0^\infty c\,\mathrm{d}t \equiv 1$$

By defining the height equivalent to a theoretical plate (H) by:

$$H = \frac{\mu_2' L}{\mu_1^2} \tag{12}$$

the Taylor–Aris model leads to the following relation:

$$H = \frac{vd^2}{96D_{1,2}} + \frac{2D_{1,2}}{v} \tag{13}$$

which is identical to Golay's equation for an unretained component[17].

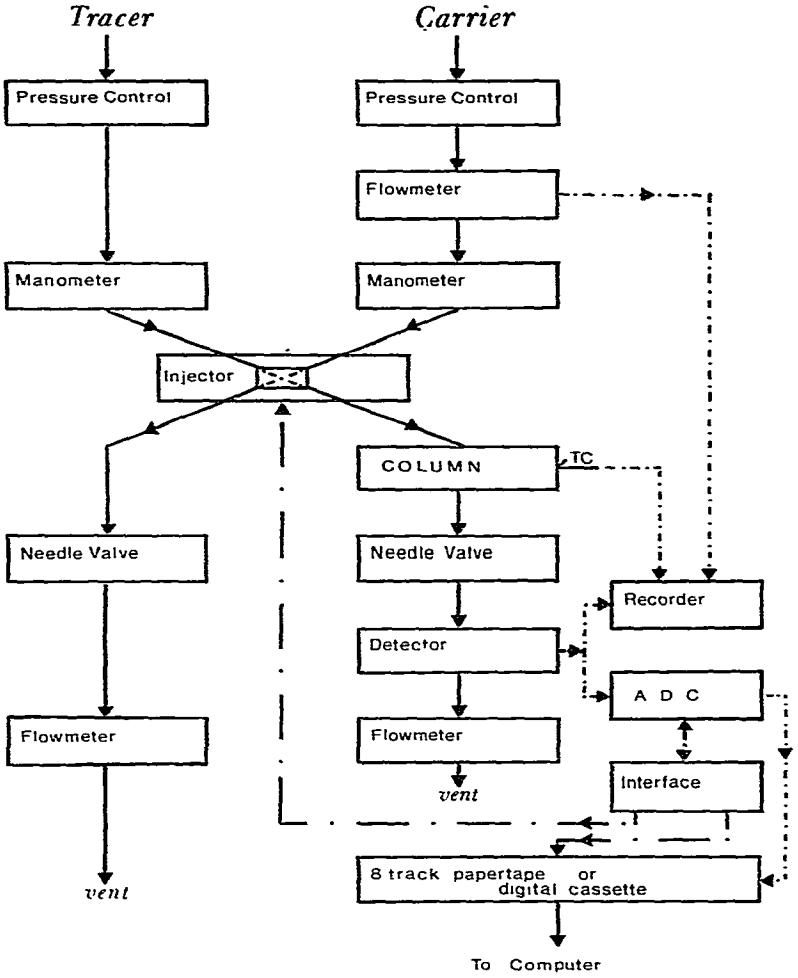

Fig. 2. Experimental set-up.

EXPERIMENTAL

The measurements were performed in the apparatus shown schematically in Fig. 2. To minimize the so-called extra-column effects, the dead volumes were kept as small as possible. All tubing from the injector to the detector was made from 1.2-mm I.D. stainless-steel tubes, while the tubes under investigation were standard $\frac{1}{4}$-in. O.D. A further improvement was achieved by choosing a column pressure higher than the pressure in the detector; the pressure in the column was about 0.8 MPa (8 bar), while the pressure in the detector was atmospheric.

The trace gas was injected at the same pressure as the carrier gas in order to avoid large disturbances of the gas flow. The injection device was a pneumatically operated Carle valve (Model 2014) with an injection volume of 50 μl. The column was immersed in a water-bath.

The detector was a thermal conductivity cell (Gow-Mac). The analogue signal

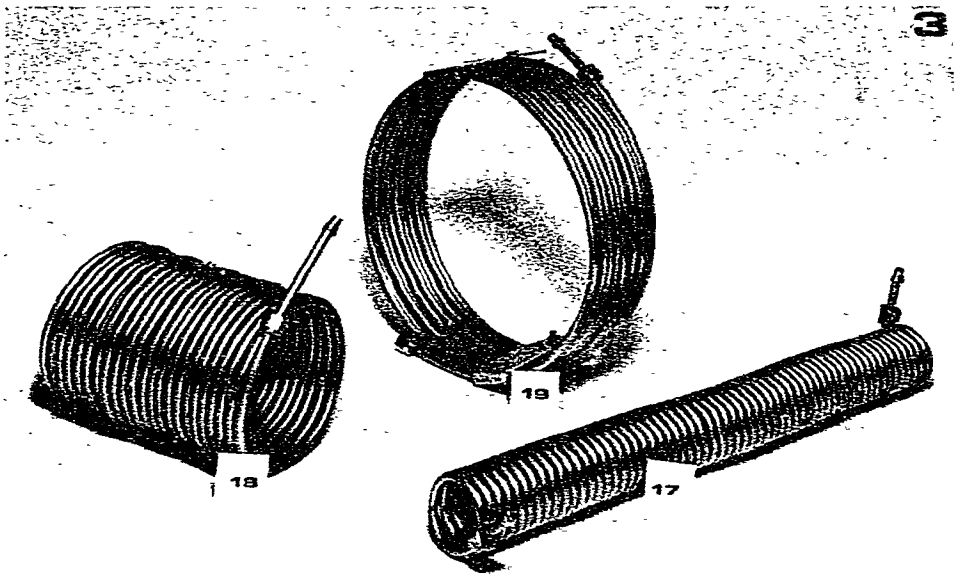

Fig. 3. Photograph of the tubes used.

TABLE I

DIMENSIONS OF TUBES USED

No.	*L* *(m)*	*d* *(10^{-3}m)*	d_c *(10^{-3}m)*	λ
17	8.086	4.72	43	9.0
18	7.846	4.79	109	22.7
19	7.526	4.79	227	47.3

from the thermal conductivity cell, in addition to being registered on a recorder, after sampling was converted into a digital signal by means of a digital voltmeter (Hewlett-Packard, Model 3480B) and punched on paper tape or written on a digital cassette.

Fig. 3 is a photograph of the tubes used and Table I gives the dimensions.

The moments of the peaks were calculated by means of Simpson integration, except the tail of the curve, which was approximated by an exponential decay function

TABLE II

DESIGN OF THE EXPERIMENTS

Pr = propene; Fr = Freon-13.

System	*Sc*	λ	*Re*	*Symbol*
He → N_2	0.23	9.0	10–700	◆
Kr → N_2	1.13	9.0	10–800	●
N_2 → He	1.75	9.0; 22.7; 47.1	2–200	▲; ○; ◇
Pr → He	2.79	9.0	1–100	■
Fr → He	3.02	9.0	2–100	★

and analytically integrated[16]. As the injection of tracer gas and the sampling of the data were automated, it was easy to carry out each experiment several times under identical conditions. Such a set of experiments will be referred to as a "run"; each run represents at least three measurements.

The experiments in which *Re*, *Sc* and λ were varied are summarized in Table II; A → B means A injected into a stream of B.

RESULTS AND DISCUSSION

Observation of secondary flow phenomena in gaseous systems was made possible by continuous injection of the vapour of titanium(IV) chloride in a stream of moist air; the streams are made visible by the formation of small white particles of titanium(IV) oxide. Helices were clearly observed and, therefore, the conclusion can be drawn that gas systems also show secondary flow phenomena. The quantitative conditions and results of the dispersion measurements are given in Tables III and IV.

Fig. 4 shows the dimensionless dispersion coefficient K_c as function of *Re* for the various tracer gas–carrier gas combinations for constant λ. The theoretical curves according to the Taylor–Aris model are also given.

As might have been expected, the experimental points coincide with the Taylor–Aris solution at low *Re*. At higher values large deviations occur. It is clear that the deviations increase with increasing *Sc*. This could have been expected from results of studies in liquid systems, where the secondary flow effect is also more pronounced at higher *Sc* values[7].

TABLE III

CONDITIONS AND RESULTS FOR COLUMN 17

Temperature: 303°K.

Run	*Pressure (MPa)*	*Velocity (m/sec)*	*Re*	μ_1 *(sec)*	*S.D. (%)*	μ'_2 *(sec²)*	*S.D. (%)*
Tracer, helium; carrier, nitrogen							
800909	0.813	0.005657	13.4	1329	0.04	827.1	5.9
800910	0.809	0.01026	24.3	787.7	0.02	142.8	0.43
800907	0.807	0.01487	34.9	547.2	0.06	58.08	6.1
800908	0.806	0.03048	71.8	265.3	0.07	10.72	4.2
800911	0.804	0.04439	104.3	182.2	0.02	4.936	1.4
800912	0.802	0.06261	146.7	129.1	0.03	2.825	12
800901	0.801	0.07988	187.1	101.2	0.05	1.912	5.6
800902	0.796	0.1100	256.1	73.50	0.04	1.132	4.3
800903	0.792	0.1409	326.2	57.41	0.08	0.8129	2.6
800904	0.786	0.1776	408.3	45.52	0.12	0.5734	3.8
800905	0.781	0.2159	497.7	37.10	0.21	0.5398	3.2
800906	0.774	0.2653	600.4	30.48	0.24	0.3893	6.2
Tracer, krypton; carrier, nitrogen							
801101	0.812	0.008475	19.9	954.1	0.09	173.1	11
801102	0.810	0.02027	48.0	399.0	0.03	39.66	4.0
801103	0.809	0.03092	73.1	261.5	0.02	17.49	2.3
801104	0.806	0.04893	115.2	165.3	0.02	7.131	5.9
801105	0.804	0.06012	141.3	134.5	0.03	5.299	3.6

(Continued on p. 162)

TABLE III *(continued)*

Run	*Pressure (MPa)*	*Velocity (m/sec)*	*Re*	μ_1 *(sec)*	*S.D. (%)*	μ'_2 *(sec²)*	*S.D. (%)*
801106	0.805	0.06967	163.8	116.1	0.02	4.374	6.6
801107	0.804	0.07384	173.5	109.5	0.02	3.317	4.7
801108	0.801	0.09697	226.9	83.38	0.06	2.561	5.2
801109	0.794	0.1471	341.1	54.98	0.14	1.341	11
801110	0.790	0.1762	406.5	45.90	0.12	0.9848	12
801111	0.782	0.2291	523.4	35.29	0.26	0.6115	3.7
801112	0.775	0.2711	613.7	29.83	0.32	0.4398	5.9
801113	0.770	0.3086	694.0	26.21	0.30	0.3422	9.8
801114	0.759	0.3718	824.3	21.75	0.42	0.2543	5.8
Tracer, nitrogen; carrier, helium							
602301	0.812	0.003680	1.1	2197	0.03	8318	4.6
602302	0.811	0.008816	2.7	917.2	0.08	215.2	18
602303	0.810	0.01931	5.9	418.7	0.03	30.67	1.4
602304	0.807	0.02855	8.6	283.2	0.05	13.56	0.50
602305	0.805	0.04658	14.1	173.6	0.02	6.113	1.5
602306	0.804	0.06229	18.8	129.8	0.07	3.926	2.6
602307	0.799	0.09824	29.4	82.31	0.02	2.023	5.7
602312	0.793	0.1279	38.0	63.24	0.04	1.394	2.4
602401	0.786	0.1636	48.2	49.43	0.05	0.8744	0.58
602308	0.777	0.2415	70.3	33.48	0.03	0.3617	3.3
602310	0.760	0.3772	107.4	21.44	0.12	0.1620	6.4
602309	0.760	0.3775	107.5	21.42	0.12	0.1541	2.5
602311	0.727	0.6190	168.6	13.06	0.30	0.06271	7.9
Tracer, propene; carrier, helium							
800802	0.815	0.004801	1.5	1684	0.05	746.0	4.7
800801	0.813	0.008794	2.7	919.5	0.02	151.2	0.65
800803	0.811	0.01980	6.0	408.4	0.02	27.97	1.4
800804	0.809	0.03114	9.4	259.7	0.01	13.12	1.9
800805	0.807	0.04660	14.1	173.5	0.02	7.665	2.2
800806	0.804	0.06308	18.9	128.2	0.08	5.188	2.4
800807	0.802	0.08546	25.6	94.61	0.05	3.283	0.82
800808	0.795	0.1285	38.2	62.91	0.04	1.500	1.9
800809	0.788	0.1742	51.3	46.42	0.09	0.8321	2.8
800810	0.782	0.2175	63.5	37.18	0.06	0.5328	7.8
800811	0.772	0.2897	83.6	27.91	0.09	0.3096	2.9
800812	0.763	0.3584	102.2	22.56	0.09	0.2000	6.3
800813	0.755	0.4207	118.7	19.22	0.27	0.1660	18
Tracer, Freon-13; carrier, helium							
801011	0.814	0.007560	2.3	1070	0.34	243.1	3.2
801012	0.812	0.01123	3.4	720.2	0.03	90.27	0.30
801001	0.811	0.01924	5.8	420.2	0.04	31.78	4.9
801002	0.808	0.03207	9.7	252.1	0.02	14.69	7.3
801003	0.807	0.04875	14.7	165.9	0.02	7.811	1.3
801004	0.804	0.06616	19.9	122.2	0.03	5.192	1.5
801005	0.798	0.1029	30.7	78.56	0.07	2.642	9.0
801006	0.795	0.1343	39.9	60.21	0.05	1.527	1.4
801007	0.789	0.1821	53.7	44.41	—	0.8231	—
801008	0.784	0.2238	65.6	36.13	—	0.5617	—
801009	0.777	0.2684	77.9	30.13	0.06	0.4002	3.6
801010	0.778	0.3114	90.5	25.97	0.07	0.4200	1.9

TABLE IV

CONDITIONS AND RESULTS FOR COLUMNS 17, 18 AND 19

Tracer, nitrogen; carrier, helium.

Run	*Pressure (MPa)*	*Velocity (m/sec)*	*Re*	μ_1 *(sec)*	*S.D. (%)*	μ'_2 *(sec²)*	*S.D. (%)*
Column 17; $\lambda = 9.0$							
602301	0.812	0.003680	1.1	2197	0.03	8318	4.6
602302	0.811	0.008816	2.7	917.2	0.08	215.2	18
602303	0.810	0.01931	5.9	418.7	0.03	30.67	1.4
602304	0.807	0.02855	8.6	283.2	0.05	13.56	0.50
602305	0.805	0.04658	14.1	173.6	0.02	6.113	1.5
602306	0.804	0.06229	18.8	129.8	0.07	3.926	2.6
602307	0.799	0.09824	29.4	82.31	0.02	2.023	5.7
602312	0.793	0.1279	38.0	63.24	0.04	1.394	2.4
602401	0.786	0.1636	48.2	49.43	0.05	0.8744	0.58
602308	0.777	0.2415	70.3	33.48	0.03	0.3617	3.3
602310	0.760	0.3772	107.4	21.44	0.12	0.1620	6.4
602309	0.760	0.3775	107.5	21.42	0.12	0.1541	2.5
602311	0.727	0.6190	168.6	13.06	0.30	0.06271	7.9
Column 18; $\lambda = 22.7$							
602501	0.815	0.004487	1.4	1749	0.03	1271	1.3
602502	0.807	0.009454	2.9	829.9	0.02	185.7	0.65
602503	0.806	0.01832	5.6	428.3	0.02	33.48	0.66
602504	0.804	0.02712	8.3	289.3	0.03	14.39	0.67
602505	0.801	0.04381	13.3	179.1	0.02	6.262	0.32
602506	0.800	0.05590	17.0	140.4	0.07	4.442	0.86
602601	0.793	0.09186	27.7	85.41	0.03	2.221	1.0
602602	0.788	0.1259	37.7	62.34	0.04	1.486	1.8
602603	0.781	0.1700	50.5	46.41	0.05	0.9852	1.9
602604	0.772	0.2312	67.9	33.94	0.09	0.6216	2.5
602605	0.750	0.4029	115.0	19.47	0.13	0.2112	3.6
602606	0.717	0.6245	170.4	12.56	0.26	0.09037	8.1
Column 19; $\lambda = 47.3$							
602701	0.815	0.004231	1.3	1781	0.04	1825	1.6
602702	0.809	0.007742	2.4	973.4	0.13	304.2	0.64
602703	0.805	0.01767	5.4	426.4	0.17	34.22	0.82
602704	0.803	0.03060	9.3	246.3	0.02	11.22	0.88
602705	0.800	0.04485	13.6	168.0	0.02	5.818	0.35
602706	0.799	0.06218	18.9	121.2	0.01	3.625	0.73
602707	0.793	0.09706	29.3	77.65	0.04	2.069	2.2
602801	0.789	0.1276	38.3	59.05	0.04	1.469	2.6
602802	0.780	0.1806	53.6	41.72	0.07	0.9405	1.2
602803	0.775	0.2230	65.7	33.80	0.10	0.7536	5.4
602804	0.749	0.3994	113.8	18.87	0.14	0.2947	3.4
602805	0.715	0.6356	172.8	11.86	0.20	0.1159	12

Fig. 5 shows the results of experiments with a constant value of *Sc* and varying λ. The deviation from the Taylor–Aris solution increases with decreasing λ, which is not illogical. Secondary flow is generated by the curvature of the tube and a low value of λ means a strongly curved tube and, therefore, the largest effect of secondary flow. Fig. 5 also shows that the value of *Re* at which the deviation starts depends on λ. At low λ the deviation starts earlier than at higher values for λ.

In Fig. 6 the data in Fig. 5 are plotted against *De*. Apparently, the points

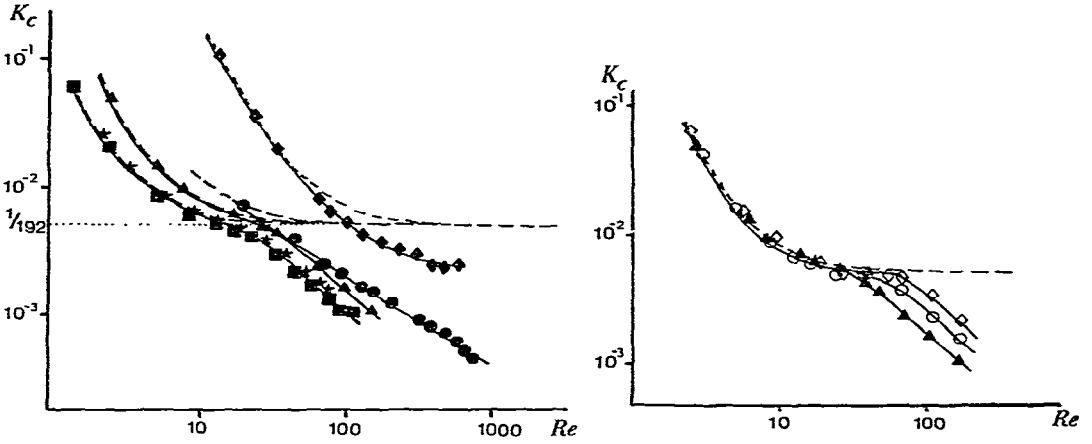

Fig. 4. Dimensionless dispersion coefficient *vs.* *Re* with varying *Sc*. Symbols defined in Table II; (--------) Taylor–Aris model.

Fig. 5. Dimensionless dispersion coefficient *vs.* *Re* with varying λ. Symbols defined in Table II; (--------) Taylor–Aris model.

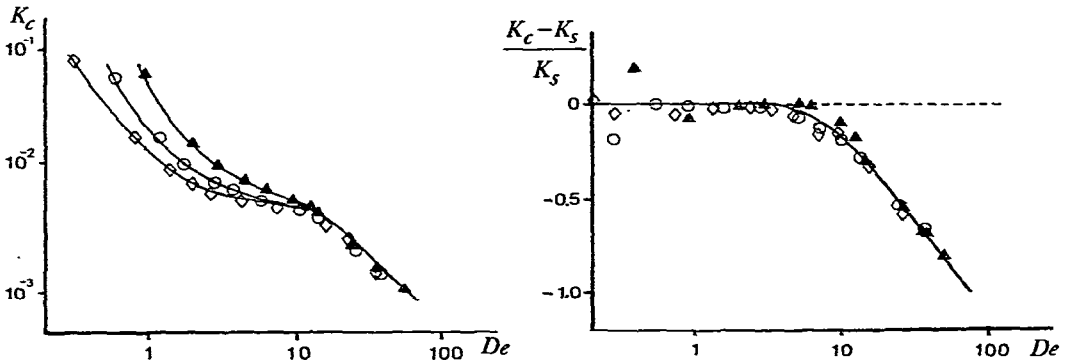

Fig. 6. Dimensionless dispersion coefficient *vs.* *De* with varying λ. Symbols defined in Table II.

Fig. 7. Normalized difference between the dimensionless dispersion coefficients for the coils and the Taylor–Aris model *vs.* *De* with varying λ. Symbols defined in Table II; (--------) Taylor–Aris model.

corresponding with experiments in which secondary flow is important lie on a single curve. Hence the effect of curvature is completely accounted for by the Dean group, which is in agreement with results with liquids flowing through coils[7]. In the low *Re* region, the Taylor–Aris model holds and therefore the points which lie on a single curve in Fig. 5 now lie on three different curves. An elegant means of presenting these results is to plot the normalized difference $(K_c-K_s)/K_s$ as function of *De*, and Fig. 7 shows this plot for the measurements with varying λ. All points now form one curve. The scattering at the lowest velocities is inherent to the measuring technique. At very low velocities, the absolute height of the signal decreases, which results in a loss of reliability, especially of the second moment. Fig. 7 illustrates the usefulness of the groups K_c, K_s and *De*.

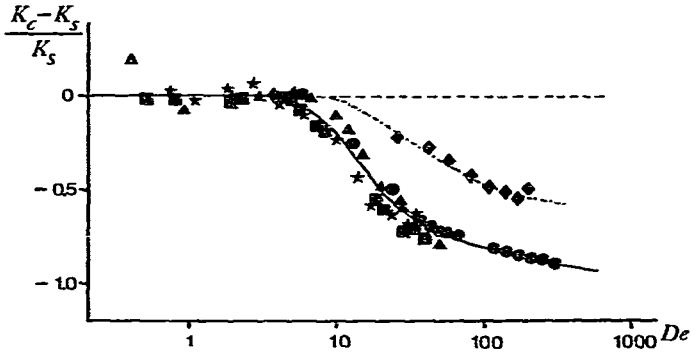

Fig. 8. Normalized difference between the dimensionless dispersion coefficients for the coils and the Taylor–Aris model *vs.* *De* with varying *Sc*. Symbols defined in Table II; (--------) Taylor–Aris model.

In Fig. 8, $(K_c-K_s)/K_c$ against *De* is shown for the measurements with varying *Sc*. Here, the experimental points are not completely correlated by *De*. In Fig. 9 the data are plotted against $De\sqrt{Sc}$. For moderate values of $De\sqrt{Sc}$ the points lie close together, but for higher $De\sqrt{Sc}$ values large deviations are observed, although smaller than in Fig. 8. These results agree closely with those of Janssen[10], who found that for $De\sqrt{Sc} < 10$ the Taylor–Aris model holds.

The advantageous effect of coiling can be appreciated from a plot of the height equivalent to a theoretical plate (H) against the linear velocity, and Fig. 10 gives the results for varying λ and constant *Sc*. Again, it can be seen that at low velocities the Taylor–Aris model is followed. At higher velocities a remarkable decrease in H takes place. This decrease is more important the lower the value of λ, and in this region it is therefore possible to increase the velocity of the carrier gas without increasing H. This result offers the possibility of rapid separations. Of course, in practice the stationary phase will not allow unlimitedly high velocities because at high velocities the rate of mass transfer in the stationary phase will determine the separation performance. Moreover, the contribution of the velocity profile to the height equivalent to a theoretical plate drastically increases with increasing retention, as is shown,

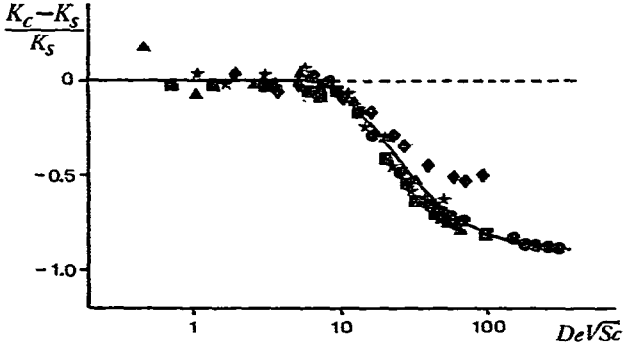

Fig. 9. Normalized difference between the dimensionless dispersion coefficients for the coils and the Taylor–Aris model *vs.* $De\sqrt{Sc}$ with varying *Sc*. Symbols defined in Table II; (--------) Taylor–Aris model.

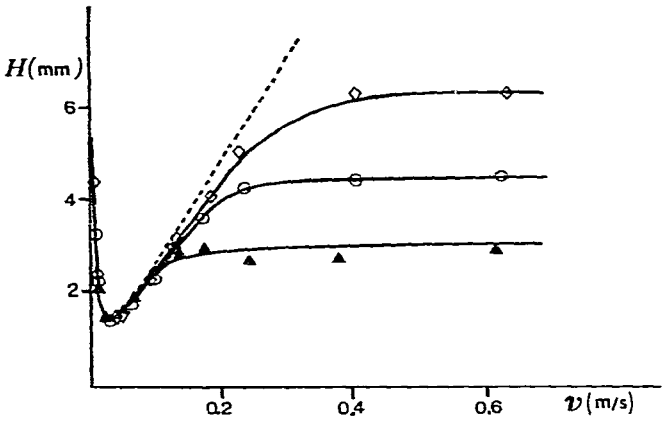

Fig. 10. Height equivalent to a theoretical plate as a function of the mean velocity with varying λ. (———) Taylor–Aris solution.

e.g., by Golay's equation. However, this work shows that, apart from retention, the contribution of mass transfer in the mobile phase to the height equivalent to a theoretical plate for coiled tubes is much less than for straight tubes. This reduction amounts to a factor of 4–10 at the highest velocities used in this study.

CONCLUSIONS

(1) At low velocities, coiled tubes and straight tubes show dispersion behaviour identical with that described by the Taylor–Aris equation.

(2) At high velocities, the dispersion in coiled tubes is less than in straight tubes. The difference is a function of the Dean and Schmidt groups.

(3) The Taylor–Aris equation holds for $De\sqrt{Sc} < 10$.

REFERENCES

1 W. R. Dean, *Phil. Mag. II*, 4 (1927) 208.
2 J. A. Koutsky and R. J. Adler, *Can. J. Chem. Eng.*, 42 (1964) 239.
3 E. van Andel, H. Kramers and A. de Voogd, *Chem. Eng. Sci.*, 19 (1964) 77.
4 R. J. Nunge, T.-S. Lin and W. N. Gill, *J. Fluid Mech.*, 51 (1972) 363.
5 L. R. Austin and J. D. Seader, *AIChE J.*, 19 (1973) 85.
6 R. N. Trivedi and K. Vasudeva, *Chem. Eng. Sci.*, 29 (1974) 2291.
7 R. N. Trivedi and K. Vasudeva, *Chem. Eng. Sci.*, 30 (1975) 317.
8 R. Tijssen, *Chromatographia*, 3 (1970) 525.
9 R. Tijssen and R. T. Wittebrood, *Chromatographia*, 5 (1972) 286.
10 L. A. M. Janssen, *Chem. Eng. Sci.*, 31 (1976) 215.
11 F. Doué, J. Merle d'Aubigne and G. Guiochon, *Chim. Anal. (Paris)*, 53 (1971) 363.
12 J. F. M. Kolk, *Ph.D. Thesis*, Amsterdam, 1977.
13 G. I. Taylor, *Proc. Roy. Soc. (London)*, A219 (1953) 186.
14 R. Aris, *Proc. Roy. Soc. (London)*, A235 (1956) 67.
15 S. Goldstein (Editor), *Modern Developments in Fluid Dynamics*, Vol. 1, Dover, New York, p. 84.
16 M. F. Edwards and J. F. Richardson, *Chem. Eng. Sci.*, 23 (1968) 109.
17 O. E. Schupp III, *Gas Chromatography*, Interscience, New York, 1968.